Ultrafast Photophysical Studies of a Multicomponent Sunscreen: Oxybenzone – Titanium Dioxide Mixtures

Lewis A. Baker[a], Lucy C. Grosvenor[a], Michael N. R. Ashfold[b], Vasilios G. Stavros[a,*]

[a]*Department of Chemistry, University of Warwick, Gibbet Hill Road, Coventry, CV4 7AL, United Kingdom.*
[b]*School of Chemistry, University of Bristol, Cantock's Close, Bristol, BS8 1TS, United Kingdom.*

Abstract

Recent studies of the sunscreen constituent oxybenzone have suggested that the dominant mechanism underlying the efficient photoprotection it offers relies on an initial ultrafast *enol* → *keto* tautomerisation, followed by nonadiabatic transfer to the ground electronic state. Subsequent collisions with the solvent bath then reform the original *enol* tautomer. Utilising femtosecond transient electronic absorption spectroscopy we explore the dissipation of electronic excitation energy in oxybenzone in the presence of titanium dioxide, a widely used, and complementary sunscreen component. We find the relaxation dynamics of this popular organic filter are unaltered by the presence of this favoured inorganic scatterer and the overall dynamics can be described by the additive contribution of the individual constituents. The combination of the two components provides broadband photoprotective properties justifying the widely used organic filter and inorganic scatterer mixtures in commercial sunscreen products.

Keywords: Oxybenzone, Titanium dioxide, Sunscreens, Transient absorption spectroscopy, Ultrafast photochemistry, Solution phase

1. Introduction

Vitamin D is an important biological precursor for various hormones which regulate biochemical tasks *e.g.* calcium absorption. A deficiency in vitamin D has been linked to multiple aliments including rickets and osteoporosis [1, 2]. More than 90% of metabolised vitamin D in the body is synthesised *via* the ultraviolet-B (UV-B, 315-280 nm) mediated conversion of 7-dehydrocholesterol to previtamin D3 [3, 4]. Thus UV radiation (UVR) and, in particular, UV-B is essential for good health. On the other hand, too much exposure to UVR can have adverse consequences, the most fatal being the development of malignant melanoma [5]. The body is therefore in a delicate balance of the so called *burden of disease*, too much UV exposure and sensitive tissues are damaged, too little and not enough vitamin D is synthesised [6]. The body has evolved to maintain this balance through the development of UV-absorbing melanins distributed throughout the skin that intercept UVR before it reaches these sensitive tissues. The number of melanins and their distribution are regulated through melanogenesis [7], which is up-regulated in environments of high UV exposure or down-regulated in low UV environments in order to maintain an optimal equilibrium in the burden of disease. This however is a delayed process, where any interim response affords little

additional photoprotection [8]. An almost universal solution to this has been the development of sunscreens which act to complement natural photoprotection [9–13].

Sunscreens are applied to the upper epidermis of the skin and work by absorbing or scattering harmful UV wavelengths (typically <340 nm) generally through two methods. Organic filters are typically aromatic molecules which absorb UVR and dissipate it through ultrafast pathways. Examples include avobenzone [14, 15], oxybenzone [16–19] and octocrylene [20]. Inorganic scatterers, in addition to absorption, also operate by scattering UV radiation away. Prominent examples include titanium dioxide (TiO_2) and zinc oxide [21, 22]. TiO_2, in particular, is also attracting widespread interest in terms of TiO_2-dye photophysics [23, 24]. Most studies of the photoprotection properties of these sunscreen components have focused on individual filters in isolation, but commercial sunscreen products typically contain tens of components in order to produce an efficient, broadband photoprotective and aesthetically pleasing product. In this study we focus on oxybenzone *and* titanium dioxide, two sunscreen constituents which are often combined to provide broad spectral coverage and efficient photoprotection, to understand if the previously observed photodynamics in oxybenzone are changed [16–18] by the presence of the inorganic scatterer. Figure 1 shows the overall relaxation mechanism of oxybenzone. Multi-molecular compositions have already been shown to display photodynamics different to that of the individual constituents, for example, octocrylene is known to behave as a photostabiliser to avobenzone when in solution to-

*Corresponding author
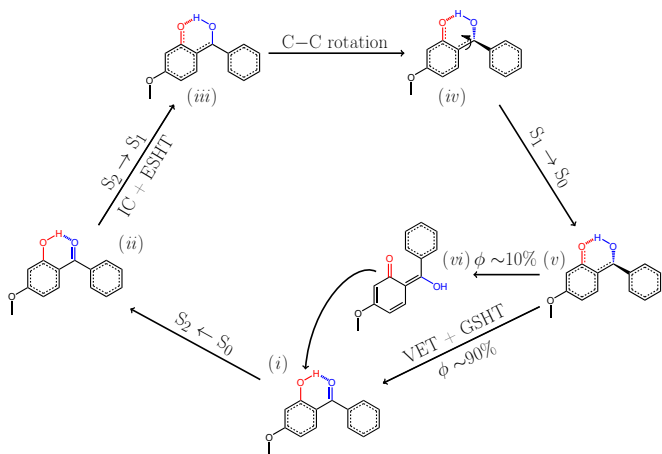Email address:* V.Stavros@warwick.ac.uk (Vasilios G. Stavros)

Figure 1: Overall relaxation mechanism of UV photoexcited oxybenzone as has been previously proposed [16, 17]. (*i*) Initial UV photoexcitation populates the $S_2(1^1\pi\pi^*)$ state (*ii*). Excited state hydrogen transfer (ESHT) to the *keto*-tautomer and internal conversion couple oxybenzone to the $S_1(1^1n\pi^*)$ state (*iii*). Rotation about the aliphatic C−C bond (*iv*) couples S_1 back to the ground S_0 state (*v*) where vibrational energy transfer (VET) to the surrounding solvent and ground state hydrogen transfer (GSHT) reforms the original *enol*-tautomer, or (*vi*) extended rotation can lead to a trans *keto*-tautomer photoproduct, with an estimated yield of ∼10% based on transient vibrational absorption measurements [16].

gether [25]. Here we explore the photophysical interdependency (or otherwise) of the individual components within an organic molecule/inorganic scatterer blend.

Given the widespread use of sunscreens in everyday life, it is somewhat surprising how little is known about the underlying mechanisms of energy flow, or photoprotection, on a molecular level [13]. Tracking the energy flow in real time can provide crucial insight into the underlying mechanisms that drive photoprotection and/or photostability. To this end, we utilise femtosecond pump-probe transient electronic (UV-visible) absorption spectroscopy (TEAS) to study how the excited state dynamics of an organic filter are altered, *if at all*, whilst in the presence of a potential perturber, a step up in the complexity of understanding the behaviour of commercial sunscreen products. Here, the organic filter is oxybenzone and the perturber is TiO_2.

2. Experimental Methodology

Sample preparation. For all TEAS measurements, samples of oxybenzone (OB, 98%, Sigma-Aldrich), TiO_2 nanoparticles (>99%, ∼21 nm diameter, *P25*, Sigma-Aldrich) and the combination of the two, TiO_2:OB in dioxane (≥99%, Fisher Scientific) or methanol (≥99.6%, Sigma-Aldrich), were made. For all solutions containing OB, 10 mM was used. For dispersions containing TiO_2, 1 mM and 25 mM (for full saturation) in methanol were used. In dioxane, 1 mM was sufficient for saturation. These ratios were chosen for the extreme ends of what might exist in a commercial product [26]. All samples were

made to 50 mL for use in recirculation in TEAS measurements, and were made to 5 mL for all UV-visible measurements. Water was omitted as a solvent due to OBs poor solubility. Samples are from hereon referred to as; OB-D (10 mM oxybenzone in dioxane), TiO_2:OB-D (1 mM TiO_2 with 10 mM OB in dioxane), 1 mM-TiO_2:OB-M (1 mM TiO_2 with 10 mM OB in methanol) and 25 mM-TiO_2:OB-M (25 mM TiO_2 with 10 mM OB in methanol). All 'steady state' UV-visible spectra are taken with either a Cary 50 or Cary 1E UV-visible spectrophotometer, with a 1 cm path length quartz cuvette (see SI for details), and are shown in Figure 2.

Pump-probe setup. The TEAS setup employed in this study is detailed in Reference [28]. Briefly, samples containing OB were photoexcited at 325 nm, while those containing TiO_2 only were photoexcited at 330 nm (see UV-visible absorption maxima, Figure 2). The pump pulses have fluences of ∼1-2 mJ·cm^{-2} and are produced by a commercial optical parametric amplifier (TOPAS-C, Light Conversion) seeded by a 1 kHz pulse train (1 W, 800 nm) from a Ti:sapphire chirp regenerative amplifier (Spitfire Pro XP, Spectra Physics). A small portion of this 800 nm fundamental is used to produce a broadband white light continuum *via* nonlinear processes in a 1 mm thick CaF_2 window, which is used as the probe in the region of ∼335–675 nm. A half-wave plate is used to hold the probe polarisation at the magic angle (54.7°) relative to the pump polarisation. Samples are recirculated between two CaF_2 windows with 100 μm PTFE spacers *via* a flow-through cell (Harrick Scientific) from a 50 mL reservoir to ensure a fresh sample for each pump-probe measurement.

Analysis. Each recorded transient absorption spectrum (TAS) is first chirp corrected using the KOALA package
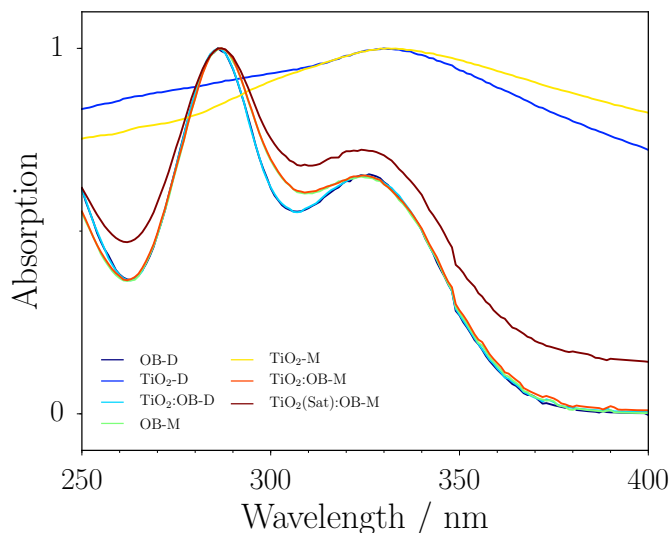

Figure 2: UV-visible spectra of OB, TiO_2 and OB-TiO_2 in dioxane (D) and methanol (M). Each spectrum is normalised to its respective maximum. The TiO_2 profiles are convolutions of both absorption and scattering contributions [27]. Raw, unnormalised spectra, and concentrations are given in the SI.
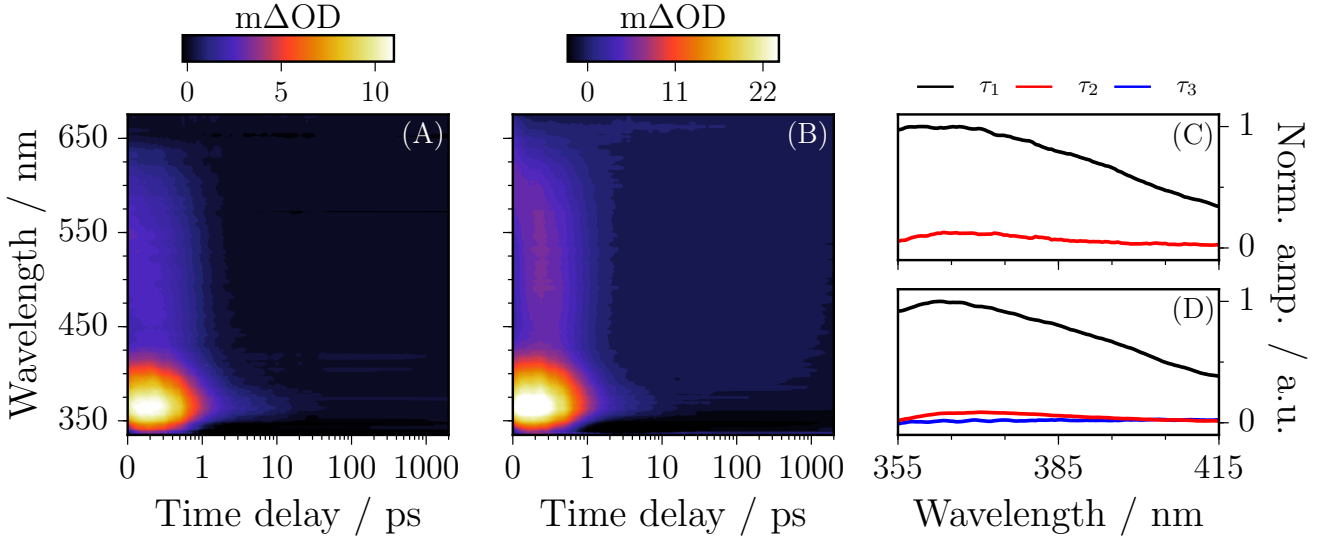
Figure 3: Raw TAS of (A) OB-D and (B) TiO$_2$:OB-D following 325 nm photoexcitation, the colourmap indicates the change in optical density (ΔOD) and is scaled logarithmically with Δt. (C) The corresponding DAS for OB-D as determined by the global fitting procedure for the two lifetimes detailed in Table 1. (D) Similarly for TiO$_2$:OB-D with three lifetimes. Fitting excludes early delay times to avoid the instrument response function, see SI for details.

[29]. Then a global fitting procedure is used to extract dynamic lifetimes from each TAS [30]. In this global fitting procedure, the experimentally recorded TAS is modelled as the sum of n exponential functions:

$$\mathcal{F}(\lambda, \Delta t) = \sum_i^n A_i(\lambda) e^{\frac{-(\Delta t - t_0)}{\tau_i}}, \qquad (1)$$

where $A_i(\lambda)$ is the decay associated spectrum (DAS) for the ith-exponential decay function with lifetime τ_i, and t_0 denotes the temporal position of the pump-probe pulse overlap, where the pump-probe time delay is denoted by Δt. The sum of squares, $\mathcal{F}(\lambda,\Delta t)$, of the modelled TAS are minimised with respect to the experimentally measured TAS. For all TAS, $n = 2$, or $n = 3$ if one exponential has a long lifetime. All confidence intervals assigned to lifetimes are reported to the 95% level using support plane analysis [31] (see supplementary information, SI). All global fits include probe spectral regions between 355–415 nm which encompasses the main absorption feature of OB, and begin at a large enough Δt so that convolution with an instrument response function is not necessary (see SI). This procedure closely follows that used in previous studies on OB solutions alone [16, 17].

3. Results

Measurements of TiO$_2$ only in methanol (both concentrations) and in dioxane following photoexcitation at the UV-visible absorption maximum (330 nm) are reported in the SI. Minimal dynamics are seen, all of which occur within the temporal resolution of the experimental instrument response function ($\sim$100 fs, [17]), except for

when using 25mM-TiO$_2$-M where a strong negative signal is observed which does not fully recover by the maximum available pump-probe delay time of 2 ns. Comparing the spectral location of the negative signal to the UV-visible spectrum of TiO$_2$, this signal can be attributed to a ground state bleach (GSB), which we return to discuss.

TAS for OB-D and TiO$_2$:OB-D following photoexcitation at 325 nm are given in Figure 3. The TAS for OB-D (Figure 3A) shows three features. (i) A negative going signal below 355 nm which, through comparison with the UV-visible spectrum of OB (Figure 2) is assigned to a GSB. (ii) An intense positive going signal centred $\sim$365 nm, which decays to the baseline by $\sim$50 ps. (iii) A broad positive signal spanning the probe spectral region $\sim$425–650 nm which decays within $\sim$2 ps. Both positive signals are assigned to excited state absorptions (ESAs) through comparison to previous measurements [16, 17], and *ab initio* calculations of similar systems [19] which likely originate from transitions to a myriad of electronics states *i.e.* $S_n \leftarrow S_1$. Similar features are observed for the TAS of TiO$_2$:OB-D, with the negative feature (i) appearing more strongly and spectrally broadened. We note that the apparent broadening is consistent with the addition of the TiO$_2$ (most clearly seen for the 25 mM-TiO$_2$ measurements, see SI).

Global fitting is employed in order to quantify the dynamical processes revealed in the TAS. The results of global fitting are summarised in Table 1. Two exponential decay functions were required (*i.e.* $n = 2$, *cf.* Eq. 1) to describe the TAS over the probe spectral region of 355–415 nm, which centres on the intense absorption feature (ii). Very early time delays ($<$300 fs) were omitted to avoid convolution with our instrument response as well
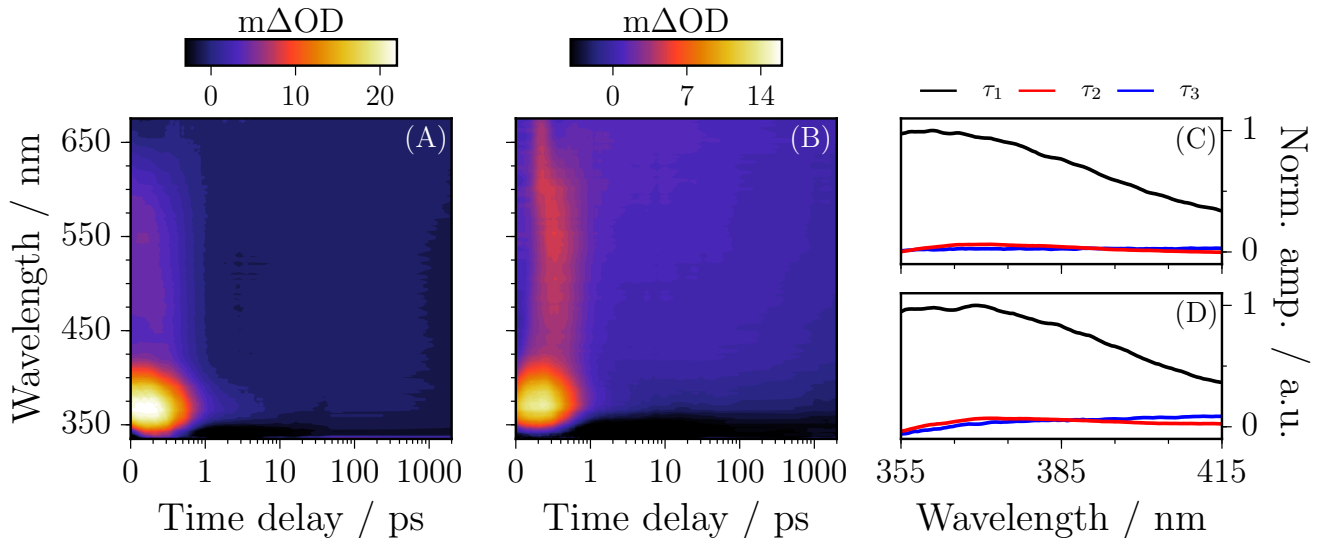
3

Figure 4: Raw TAS of (A) 1 mM-TiO$_2$:OB-M and (B) 25 mM-TiO$_2$:OB-M following 325 nm photoexcitation, the colourmap indicates the change in optical density (ΔOD) and is scaled logarithmically with Δt. (C) The corresponding DAS for 1 mM-TiO$_2$:OB-M as determined by the global fitting procedure for the three lifetimes detailed in Table 1. (D) Similarly for 25 mM-TiO$_2$:OB-M. Fitting excludes early delay times to avoid the instrument response function, see SI for details.

as a broad feature around time zero (see SI). This analysis reveals two dynamical lifetimes $\tau_1 = 537 \pm 20$ fs and $\tau_2 = 8.3 \pm 3.3$ ps with corresponding DAS shown in Figure 3C, which agree well with previous studies of OB in the nonpolar solvent cyclohexane ($\tau_1 = 375 \pm 13$ fs and $\tau_2 = 7.8 \pm 2.8$ ps) [16]. The difference in τ_1 between dioxane measurements and the previously reported cyclohexane and methanol measurements [16] may be understood by the differences in solvent viscosity (*vide infra*).

The TAS for TiO$_2$:OB-D shown in Figure 3B displays the same features as for OB-D with this addendum. A third lifetime, attributed to the additional negative contribution from the presence of the TiO$_2$ (see SI), was required to describe these TAS. This has the effect of creating a long-lived baseline offset which this third lifetime ($\geq$2 ns) captures, labelled τ_3. Once again omitting early delay times ($\Delta t <250$ fs), the other lifetimes are determined to be $\tau_1 = 575 \pm 18$ fs and $\tau_2 = 6.9 \pm 2.8$ ps which correspond very closely to the OB-D measurements.

Next we consider the solvent methanol. Previous measurements determined that OB-M displays two dynamical features, analogous to those discussed for OB-D, with lifetimes $\tau_1 = 368 \pm 13$ fs and $\tau_2 = 4.9 \pm 1.9$ ps [16], and thus

Table 1: Summary of dynamical lifetimes as determined from the global fitting for all samples (D = dioxane, M = methanol). OB-M lifetimes taken from Reference [16].

Sample	τ_1 / fs	τ_2 / ps	τ_3 / ns
OB-D	537 ± 20	8.3 ± 3.3	–
OB-M	368 ± 13	4.9 ± 1.9	–
1 mM-TiO$_2$:OB-D	575 ± 18	6.9 ± 2.8	$\geq$2 ns
1 mM-TiO$_2$:OB-M	357 ± 9	4.8 ± 1.8	$\geq$2 ns
25 mM-TiO$_2$:OB-M	363 ± 11	3.0 ± 1.4	$\geq$2 ns

provides a point of comparison when TiO$_2$ is included. For low concentrations, 1 mM-TiO$_2$:OB-M, Figure 4A, similar spectral features are seen in the TAS as in the dioxane measurements. Global fitting reveals three dynamical lifetimes, $\tau_1 = 357 \pm 9$ fs, $\tau_2 = 4.8 \pm 1.8$ ps and the long lifetime $\tau_3 \geq$2 ns. The corresponding DAS are given in Figure 4C. For saturated concentrations, 25 mM-TiO$_2$:OB-M, Figure 4B, the dynamics of TiO$_2$ are much more clearly observed, see SI, whereby the long-time recovery of the GSB persists for the duration of the experiment. Global fitting reveals three lifetimes, $\tau_1 = 363 \pm 11$ fs, $\tau_2 = 3.0 \pm 1.4$ ps and $\tau_3 \geq$2 ns. For both measurements including TiO$_2$, other than the appearance of the long-lived recovery of the TiO$_2$ which requires the third lifetime, τ_1 and τ_2 compare very closely with OB-M measurements *cf.* Table 1.

4. Discussion and Conclusions

We can begin to rationalise the features in our measured TAS and assign dynamical processes to the lifetimes determined from global fitting of the TAS by drawing on both *ab initio* calculations and previous ultrafast measurements [16, 17, 19]. Considering OB-D first, the dynamics observed follow closely those of OB-M and OB-cyclohexane [16]; initial 325 nm photoexcitation populates the S$_2$ state from the ground state, S$_0$. Following this, OB undergoes internal conversion (IC) to the S$_1$ state, followed by an excited state hydrogen transfer (ESHT) along the O−H stretch, forming the *keto* tautomer. This cascade of processes is captured by the broad absorption feature which is not considered in the global fit, and resides, heavily convoluted, within the instrument response of the experiment of ~100 fs, which in accord with other *enol-keto* driven

systems [32] and has been confirmed recently *via* trajectory surface hopping calculations [33]. Rotation about the aliphatic C−C bond is required in order to couple the S_1 S_0 states, resulting in a twisted *keto* geometry and enables population transfer through a conical intersection (CI) between the S_1 and S_0 potential energy surfaces (PESs), shown in Figure 1. These processes are captured by the lifetime τ_1. This assignment also accounts for the difference in the τ_1 lifetime between solvents, which may be understood through differences in the solvent viscosity, η. Dioxane exhibits a greater viscosity compared to cyclohexane or methanol ($\eta = 1.19$, 0.897 and 0.551 mPa·s respectively [34]) and is therefore likely to offer greatest friction to the geometry change required before OB can couple to its S_0 state [35].

The twisted *keto* species is not stable on the S_0 PES, and there are two routes *via* which it may relax. (*i*) The ground state may recover through a reverse tautomerisation involving a ground state hydrogen transfer reforming the *enol* tautomer, which further relaxes by vibrational energy transfer (VET) to the surrounding solvent molecules. (*ii*) Formation of a long-lived photoproduct, most likely through extended C−C bond rotation forming a non-chelated, trans *keto* tautomer as previously reported [16]. However, a possibility remains that the photoproduct might be a phenoxyl radical [18]. The first of these routes appears dominant, given that the majority of the GSB recovers on the time scale of the experiment; the incomplete recovery is therefore attributed to the formation of a photoproduct which does not recover by the maximum time delay available of 2 ns (selected transients are given in the SI). These processes are captured by the lifetime τ_2. This lifetime also displays a solvent dependence; τ_2 is consistently shorter in the more strongly interacting (polar) solvent methanol, which is in agreement with VET driven cooling where a greater degree of hydrogen bonding enhances VET [16, 36]. That being said, it could also indicate that methanol promotes the GSHT but remains convoluted with the VET.

Considering next the TiO_2 measurements only, minimal dynamics are observed, the results of which are presented in SI. For low concentrations (1 mM), any dynamics are within the instrument response or are well within the signal to noise of the experiment (<0.5 mΔOD). In methanol, where higher concentrations are achieved (25 mM), there are clear dynamics which persist to the maximum pump-probe time delays. These observations are consistent with previous studies on isolated TiO_2 nanoparticles in solution [37–39]. In the low concentration regime, TiO_2 displays ultrafast relaxation, likely through the generation and subsequent trapping of surface electrons. At higher concentrations, TiO_2 begins to behave more like a thin film, where deep trapping of electrons equilibrating between surface and shallow trapping sites occurs over 100's of ps [39].

Having characterised the dynamics displayed by each component, individually, we now discuss the measurements for the multicomponent systems. For 1 mM

TiO_2:OB-D, the TAS (Figure 3B) appears to be a simple weighted sum of the isolated OB and TiO_2 systems, with the requirement of the third lifetime accounting for the long-lived dynamics of TiO_2. This is further evidenced by similar τ_1 and τ_2 lifetimes for the individual and multicomponent systems (within 2σ of each other). Very similar conclusions are reached for both the 1 mM-TiO_2:OB-M and 25 mM-TiO_2:OB-M systems where all lifetimes are again within 2σ of their OB-M counterparts. The effect of the presence of TiO_2 in low (or saturated) concentrations on the overall dynamics is simply additive; the presence of one appears not to affect the relaxation dynamics of the other component.

To conclude, the relaxation dynamics of the popular organic filter oxybenzone in commercial sunscreens are unaltered by the presence of the widely utilised scattering (and absorptive) additive TiO_2. Unlike other additives such as photostabilisers which are known to enhance the photostability of an organic filter, TiO_2 is shown to have minimal impact on the dynamics displayed by the organic filter. This implies, at the very least, very little or no interaction between the two species, *e.g.* adsorption. This is an important result given the widespread use of TiO_2 in commercial sunscreen products and may justify the inclusion of both components in order to provide efficient broadband protection.

Acknowledgements

Supporting Information

TiO_2 measurements and representative additive spectrum of TiO_2 and oxybenzone are given. Global fitting details, residuals from fits, and error analysis are given. Early time transients and selected ground state bleach spectra are presented. Unnormalised UV-visible spectra.

References

[1] M. F. Holick, Vitamin D Deficiency, N. Engl. J. Med. 357 (2007) 266–281.

[2] A. W. Norman, From vitamin D to hormone D: fundamentals of the vitamin D endocrine system essential for good health, Am. J. Clin. Nutr. 88 (2) (2008) 491S–499S.

[3] M. F. Holick, Sunlight and vitamin D for bone health and prevention of autoimmune diseases, cancers, and cardiovascular disease, Am. J. Clin. Nutr. 80 (6) (2004) 1678S–1688S.

[4] J. S. Adams, M. Hewison, Update in Vitamin D, J. Clin. Endocrinol. Metab. 95 (2) (2010) 471–478.

[5] R. S. Mason, J. Reichrath, Sunlight vitamin D and skin cancer, Anticancer Agents Med. Chem. 13 (1) (2013) 83–97.

[6] R. Lucas, T. McMichael, W. Smith, B. Armstrong, Solar Ultraviolet Radiation. Global burden of disease from solar ultraviolet radiation, Environmental Burden of Disease Series, No. 13, World Health Organization, Geneva, 2006.

[7] H. Park, M. Kosmadaki, M. Yaar, B. A. Gilchrest, Cellular mechanisms regulating human melanogenesis, Cell. Mol. Life Sci. 66 (9) (2009) 1493–1506.

[8] J. P. Ortonne, Photoprotective properties of skin melanin, Br. J. Dermatol. 146 (61) (2002) 7–10.

[9] S. Q. Wang, Y. Balagula, U. Osterwalder, Photoprotection: a Review of the Current and Future Technologies, Dermatologic Therapy 23 (1) (2010) 31–47.

[10] M. E. Burnett, S. Q. Wang, Current sunscreen controversies: a critical review, Photodermatol. Photoimmunol. Photomed. 27 (2) (2011) 58–67.

[11] R. Jansen, U. Osterwalder, S. Q. Wang, M. Burnett, H. W. Lim, Photoprotection Part II. Sunscreen: Development, efficacy, and controversies, J. Am. Acad. Dermatol. 69 (6) (2013) 867.e1–867.e14.

[12] U. Osterwalder, M. Sohn, B. Herzog, Global state of sunscreens, Photodermatol. Photoimmunol. Photomed. 30 (2-3) (2014) 62–80.

[13] L. A. Baker, V. G. Stavros, Observing and Understanding the Ultrafast Photochemistry in Small Molecules: Applications to Sunscreens, Sci. Prog. 99 (3) (2016) 282–311.

[14] A. D. Dunkelberger, R. D. Kieda, B. M. Marsh, F. F. Crim, Picosecond Dynamics of Avobenzone in Solution, J. Phys. Chem. A 119 (24) (2015) 6155–6161.

[15] G. H. G. Trossini, V. G. Maltarollo, R. D. Garcia, C. A. S. O. Pinto, M. V. R. Velasco, K. M. Honorio, A. R. Baby, Theoretical study of tautomers and photoisomers of avobenzone by DFT methods, J. Mol. Model. 21 (319) (2015) 1–7.

[16] L. A. Baker, M. D. Horbury, S. E. Greenough, P. M. Coulter, T. N. V. Karsili, G. M. Roberts, A. J. Orr-Ewing, M. N. R. Ashfold, V. G. Stavros, Probing the Ultrafast Energy Dissipation Mechanism of the Sunscreen Oxybenzone after UVA Irradiation, J. Phys. Chem. Lett. 6 (8) (2015) 1363–1368.

[17] L. A. Baker, M. D. Horbury, S. E. Greenough, M. N. R. Ashfold, V. G. Stavros, Broadband ultrafast photoprotection by oxybenzone across the UVB and UVC spectral regions, Photochem. Photobiol. Sci. 14 (10) (2015) 1814–1820.

[18] M. T. Ignasiak, C. Houée-Levin, G. Kciuk, B. Marciniak, T. Pedzinski, A Reevaluation of the Photolytic Properties of 2-Hydroxybenzophenone-Based UV Sunscreens: Are Chemical Sunscreens Inoffensive?, ChemPhysChem 16 (3) (2015) 628–633.

[19] T. N. V. Karsili, B. Marchetti, M. N. R. Ashfold, W. Domcke, *Ab Initio* Study of Potential Ultrafast Internal Conversion Routes in Oxybenzone, Caffeic Acid, and Ferulic Acid: Implications for Sunscreens, J. Phys. Chem. A 118 (51) (2014) 11999–12010.

[20] L. A. Baker, M. D. Horbury, V. G. Stavros, Ultrafast photoprotective properties of the sunscreening agent octocrylene, Opt. Express 24 (10) (2016) 10700–10709.

[21] J. F. Jacobs, I. van de Poel, P. Osseweijer, Sunscreens with Titanium Dioxide (TiO_2) Nano-Particles: A Societal Experiment, Nanoethics 4 (2) (2010) 103–113.

[22] T. G. Smijs, S. Pavel, Titanium dioxide and zinc oxide nanoparticles in sunscreens: focus on their safety and effectiveness, Nanotechnol. Sci. Appl. 4 (2011) 95–112.

[23] U. Diebold, The surface science of titanium dioxide, Surf. Sci. Rep. 48 (2003) 53–229.

[24] Y. Lan, Y. Lu, Z. Ren, Mini review on photocatalysis of titanium dioxide nanoparticles and their solar applications, Nano Energy 2 (2013) 1031–1045.

[25] S. Forestier, Rationale for sunscreen development, J. Am. Acad. Dermatol. 58 (5) (2008) S133–S138.

[26] M. Lodén, H. Beitner, H. Gonzalez, D. Edström, U. Åkerström, J. Austad, I. Buraczewska-Norin, M. Matsson, H. Wulf, Sunscreen use: controversies, challenges and regulatory aspects, Br. J. Dermatol. 165 (2) (2011) 255–262.

[27] M. I. Cabrera, O. M. Alfano, A. E. Cassano, Absorption and Scattering Coefficients of Titanium Dioxide Particulate Suspensions in Water, J. Phys. Chem. 100 (51) (1996) 20043–20050.

[28] S. E. Greenough, G. M. Roberts, N. A. Smith, M. D. Horbury, R. G. McKinlay, J. M. Żurek, M. J. Paterson, P. J. Sadler, V. G. Stavros, Ultrafast photo-induced ligand solvolysis of *cis*-[Ru(bipyridine)$_2$(nicotinamide)$_2$]$^{2+}$: experimental and theoretical insight into its photoactivation mechanism, Phys. Chem. Chem. Phys. 16 (36) (2014) 19141–19155.

[29] M. P. Grubb, A. J. Orr-Ewing, M. N. R. Ashfold, KOALA: A program for the processing and decomposition of transient spectra, Rev. Sci. Instrum. 85 (6) (2014) 0641024.

[30] A. S. Chatterley, C. W. West, V. G. Stavros, J. R. R. Verlet, Time-resolved photoelectron imaging of the isolated deprotonated nucleotides, Chem. Sci. 5 (10) (2014) 3963–3975.

[31] J. R. Lakowicz, Principles of Fluorescence Spectroscopy, 3rd Edition, Springer Science+Business Media, 2006.

[32] M. Ziółek, J. Kubicki, A. Maciejewski, R. Naskrcki, A. Grabowska, Enol-keto tautomerism of aromatic photochromic Schiff base N,N'-bis(salicylidene)-p-phenylenediamine: Ground state equilibrium and excited state deactivation studied by solvatochromic measurements on ultrafast time scale, J. Chem. Phys. 124 (12) (2006) 124518.

[33] C.-X. Li, W.-W. Guo, B.-B. Xie, G. Cui, Photodynamics of oxybenzone sunscreen: Nonadiabatic dynamics simulations, J. Chem. Phys. 145 (7) (2016) 074308.

[34] G. W. Kauffman, P. C. Jurs, Prediction of Surface Tension, Viscosity, and Thermal Conductivity for Common Organic Solvents Using Quantitative Structure-Property Relationships, J. Chem. Inf. Comput. Sci. 41 (2) (2001) 408–418.

[35] M. Vengris, D. S. Larsen, M. A. van der Horst, O. F. A. Larsen, K. J. Hellingwerf, R. van Grondelle, Ultrafast Dynamics of Isolated Model Photoactive Yellow Protein Chromophores: "Chemical Perturbation Theory" in the Laboratory, J. Phys. Chem. B 109 (9) (2005) 4197–4208.

[36] J. C. Owrutsky, D. Raftery, R. M. Hochstrasser, Vibrational Relaxation Dynamics in Solutions, Annu. Rev. Phys. Chem. 45 (1994) 519–555.

[37] D. W. Bahnemann, M. Hilgendorff, R. Memming, Charge Carrier Dynamics at TiO_2 Particles: Reactivity of Free and Trapped Holes, J. Phys. Chem. B 101 (21) (1997) 4265–4275.

[38] H. N. Ghosh, J. B. Asbury, T. Lian, Direct Observation of Ultrafast Electron Injection from Coumarin 343 to TiO_2 Nanoparticles by Femtosecond Infrared Spectroscopy, Journal of Physical Chemistry B 102 (34) (1998) 6482–6486.

[39] Y. Tamaki, A. Furube, M. Murai, K. Hara, R. Katoh, M. Tachiya, Dynamics of efficient electron-hole separation in TiO_2 nanoparticles revealed by femtosecond transient absorption spectroscopy under the weak-excitation condition, Phys. Chem. Chem. Phys. 9 (12) (2007) 1453–1460.